CrossMark

# Impact of triple-material gate and highly doped source/drain extensions on sensitivity of DNA biosensors

M. Ouarghi[1] · Z. Dibi[1] · N. Hedjazi[1]

## Abstract

Gate engineering and highly doped source/drain region have been investigated to design a new DNA sensor for use in biomedical applications based on a double gate (DG) dielectric modulated (DM) junctionless (JL) metal oxide semiconductor field effect transistor (MOSFET) with triple material (TM) gate. Based on the dielectric modulation effect, DNA molecules in the nanogap cavity change due to the charge density of biomolecules, producing a change in the threshold voltage of the device. Analytical and numerical analysis was carried out to reveal the impact of physical parameters on the sensitivity of the proposed biosensor. Various characteristics, such as the surface potential, threshold voltage, and drain current were also investigated. The effectiveness of the proposed TM-DG-DM-JL-MOSFET structure with highly doped source/drain extensions is confirmed by comparison of the results with those for a conventional single-materiel (SM) gate DM-JL-MOSFET, revealing a good improvement in sensitivity and making the proposed structure an attractive solution for use in DNA-based sensor applications.

**Keywords** Biosensor · Dielectric modulation · DNA sensors · DMFET · Nanogap · Sensitivity · Triple-material gate · Gate engineering

## 1 Introduction

The use of DNA in the diagnosis of different diseases has increased rapidly since the completion of the Human Genome Project, enabling research to progress towards bioelectronics applications. This combination of biology and electronics has been promoted by the use of field-effect transistors as transducers. Indeed, their use in biomedical applications is growing rapidly due to their good performance, including rapid detection, miniaturized device size, low cost, and high sensitivity [1–6]. Research interest has also been attracted to label-free hybridization technology [7–9], and a significant number of investigations have been performed on different types of FET-based biosensors, including extended-gate FETs [10, 11], ion-selective FETs [12–15], nanowire FETs [16–21], and carbon nanotube FETs [22–24]. More recently, such work has also focused on the dielectric-modulated FET (DMFET), which is essentially based on the use of a nanogap in a traditional MOSFET structure [25–39].

A DMFET is a new MOSFET architecture in which biomolecules are fixed in a nanogap cavity located between the gate oxide and the gate [25]. The first application of this technique was based on the shift of the threshold voltage as a detection mechanism [7, 25]. When biomolecules fill the nanogap, they induce a variation in the threshold voltage because of the deviation of the dielectric constant $K$ from unity (corresponding to air) to a certain value ($K > 1$) [7, 25]. Similarly, a variation in current can be produced via the charge-pumping technique, providing information related to the specific binding process [31, 33, 35]. Several investigations have been carried out on dual- and three-material gate MOSFETs [40–50] with different metal work functions.

The aim of this study is to determine the impact of gate engineering on such a molecular biosensor. The present work considers the design of a novel long-channel DG-DM-JL-MOSFET with a three-material gate and highly-doped source/drain extensions for use in biomedical applications. To investigate systematically the impacts of gate engineering and the highly doping source/drain regions on the sensitivity of the DG-DM-JL-MOSFET device, an analytical model for

✉ M. Ouarghi
  m.ouarghi@univ-batna2.dz

  Z. Dibi
  zohirdibi@yahoo.fr

1 Laboratory of Advanced Automatic and Analysis of Systems (LAAAS), Department of Electronics, University of Batna2, 05000 Batna, Algeria

the surface potential and threshold voltage was developed then verified using numerical simulations with ATLAS-2D simulator. The results are then compared with those for a classical single-material gate structure [37] of similar dimensions, clearly revealing that the proposed design exhibits excellent sensitivity that makes it a potential candidate for use in future medical applications.

## 2 Device structure and operating mode

Figure 1 depicts the architecture of the DG-TM-DM-JL-MOSFET with highly doped source/drain extensions. The channel body is less heavily doped then the source/drain regions, so the concentration distribution is *npp/np/npp*. Besides, the device structure is divided into three regions, namely I, II, and III. Regions I and III contain cavity regions created in the gate oxide under gate 1 and gate 3, respectively, with metals M1 and M3; while region II contains gate oxide under gate 2 with metal M2. The lengths of M1, M2, and M3 are $L_1$, $L_2$, and $L_3$, respectively. The work function of M3 ($\phi_{M3} = 4.5$) is lower than that of M2 ($\phi_{M2} = 4.7$), which is lower than that of M1 ($\phi_{M1} = 5.1$). In the proposed device, M1 is towards the source side, while M3 is towards the drain side. The SiO$_2$ and TiO$_2$ in the gate oxide aim to improve the performance of the device and reduce the fringing electric field by the deposition of a high-*k* material directly on silicon [45]. The dimensions of the proposed device are presented in Table 1.

The aim of this study is to describe the influence of DNA molecules on the characteristics of these biosensors.

Since DNA is negatively charged, due to the phosphate groups present in its backbone [51], it will inject a negative charge density ($N_f$) at the SiO$_2$–air interface of the device.
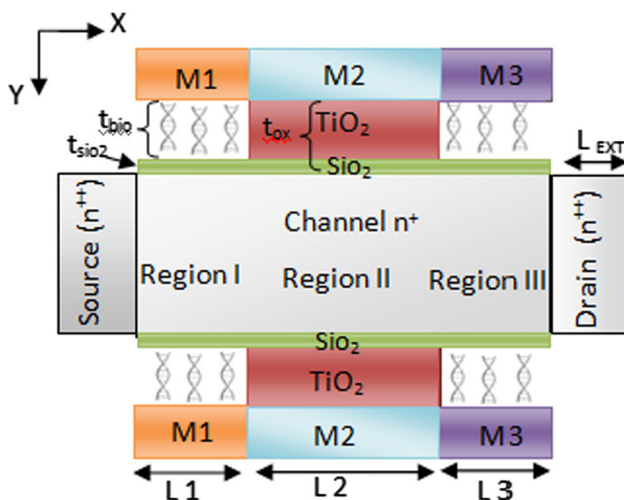


**Fig. 1** Structure of TM-DG-DM-JL-MOSFET with highly doped source/drain extensions

**Table 1** Dimensions of DG-TM-DM-JL-MOSFET with highly doped source/drain extensions

| Physical parameter | Value |
| --- | --- |
| Channel length, $L$ (nm) | 100 |
| Length of nanogap, $L_1$, $L_3$ (nm) | 25 |
| Length of gate oxide TiO$_2$, $L_2$ (nm) | 50 |
| Oxide thickness, $t_{ox1}$ (nm) | 9 |
| Silicon thickness, $t_{Si}$ (nm) | 10 |
| Nanogap thickness, $t_{bio}$ (nm) | 9 |
| Nanogap thickness, $t_{SiO2}$ (nm) | 1 |
| Doping concentration of S/D extensions, $N_{dext}$ (cm$^{-3}$) | $10^{20}$ |
| Channel doping concentration $N_d$ (cm$^{-3}$) | $10^{17}$ |

The operating mode of this biosensor is based on the presence or absence of DNA molecules in the cavity regions. When not present in the nanogap cavity, the DNA molecules are replaced by air; this fact implies the absence of the charge density $N_f$ on the one hand, and a dielectric constant of 1 on the other hand. When DNA molecules are injected into the nanogap region, the charge density ($N_f$) appears and the dielectric constant changes from 1 to $K$. Therefore, changes occur in the gate capacitance and the flat band of the device, with a corresponding variation in the threshold voltage ($v_{th}$). The sensing site of this device is the cavity region created in the gate oxide [7].

## 3 Surface potential and threshold voltage models

### 3.1 Surface potential model

The distribution of the surface potential was obtained by solving the two-dimensional (2D) Poisson equations with a parabolic approximation [52] in the silicon channel, divided into three regions:

Region I: $0 \leq Y \leq t_{Si}$; $0 < X < L_1$.

Region II: $0 \leq Y \leq t_{Si}$; $L_1 < X < L_1 + L_2$.

Region III: $0 \leq Y \leq t_{Si}$; $L_1 + L_2 < X < L$.

$$\frac{d\varphi_i(x, y)}{dx^2} + \frac{d\varphi_i(x, y)}{dy^2} = -q\frac{N_d}{\varepsilon_{Si}}, \tag{1}$$

where $i$ refers to the considered region (I, II or III), $q$ is the electron charge, $N_d$ is the doping concentration of the channel, and $\varepsilon_{Si}$ is the dielectric permittivity of silicon.

$$\varphi_i(x, y) = A_{0i}(x) + A_{1i}(x)y + A_{2i}(x)y^2, \tag{2}$$

where $A_{0i}(x)$, $A_{1i}(x)$, and $A_{2i}(x)$ are determined by using the boundary conditions and continuity of the electric flux.

At Si–SiO$_2$ interfaces, the following hold:

$$\varphi_i(x, 0) = \varphi_{\text{Si}}(x), \tag{3-a}$$

$$\varphi_i\left(x, \frac{t_{\text{Si}}}{2}\right) = \varphi_{ci}(x), \tag{3-b}$$

$$\frac{\partial \varphi_i(x, 0)}{\partial y} = \frac{C_i}{\varepsilon_{\text{Si}}}\left(\varphi_{\text{Si}}(x) - V_{\text{gs}} + V_{\text{fbi}}\right), \tag{3-c}$$

$$\frac{\partial \varphi_i(x, t_{\text{Si}})}{\partial y} = -\frac{C_i}{\varepsilon_{\text{Si}}}\left(\varphi_{\text{Si}}(x) - V_{\text{gs}} + V_{\text{fbi}}\right), \tag{3-d}$$

$$\frac{\partial \varphi_i\left(x, \frac{t_{\text{Si}}}{2}\right)}{\partial y} = 0, \tag{3-e}$$

where $\varphi_{\text{Si}}(x)$ is the surface potential, $\varphi_{ci}(x)$ is the central potential, $V_{\text{gs}}$ is the gate-to-source voltage, and $V_{\text{fbi}}$ denotes the flat-band voltage, given by

$$V_{\text{fb1}} = \phi_{\text{M1}} - \phi_{\text{Si}} - \frac{qN_f}{C_{\text{bio}}}, \tag{4-a}$$

$$V_{\text{fb2}} = \phi_{\text{M2}} - \phi_{\text{Si}}, \tag{4-b}$$

$$V_{\text{fb3}} = \phi_{\text{M3}} - \phi_{\text{Si}} - \frac{qN_f}{C_{\text{bio}}}, \tag{4-c}$$

$$\phi_{\text{Si}} = \chi_{\text{Si}} + \frac{E_g}{2}, \tag{5}$$

$$C_{\text{bio}} = \frac{\varepsilon_{\text{bio}}}{t_{\text{bio}}}, \tag{6-a}$$

$$C_1 = C_3 = \frac{C_{\text{bio}} \cdot C_{\text{SiO}_2}}{C_{\text{bio}} + C_{\text{SiO}_2}}, \tag{6-b}$$

$$C_{\text{SiO}_2} = \frac{\varepsilon_{\text{SiO}_2}}{t_{\text{SiO}_2}}, \tag{6-c}$$

$$C_2 = C_{\text{ox}} = \frac{\varepsilon_{\text{ox}}}{t_{\text{ox}}}, \tag{6-d}$$

with $t_{\text{ox}} = t_{\text{ox1}} + t_{\text{ox2}}\frac{\varepsilon_{\text{ox1}}}{\varepsilon_{\text{ox2}}}$.

$C_{\text{bio}}$ is the capacitance of the cavity region, and $C_i$ is the gate capacitance per unit area of the gate dielectric of the TM-JL-DG-MOSFET. $N_f$ and $\varepsilon_{\text{bio}}$ are, respectively, the charge density and the permittivity of the DNA molecules.

$$A_{0i}(x) = \varphi_{\text{Si}}(x), \tag{7-a}$$

$$A_{1i}(x) = \frac{C_i}{\varepsilon_{\text{Si}}}\left(\varphi_{\text{Si}}(x) + V_{\text{fbi}} - V_{\text{gs}}\right), \tag{7-b}$$

$$A_{2i}(x) = -\frac{C_i}{t_{\text{Si}}\varepsilon_{\text{Si}}}\left(\varphi_{\text{Si}}(x) + V_{\text{fbi}} - V_{\text{gs}}\right). \tag{7-c}$$

Substituting the expressions for $A_{0i}(x)$, $A_{1i}(x)$, and $A_{2i}(x)$ into (2), Eq. (1) leads to a one-dimensional second-order differential equation:

$$\frac{\partial^2 \varphi_{\text{Si}}(x)}{\partial x^2} - \alpha_i \varphi_{\text{Si}}(x) = \beta_i, \tag{8}$$

where

$$\alpha_i = \frac{8C_i}{4t_{\text{Si}}\varepsilon_{\text{Si}} + C_i t_{\text{Si}}^2}, \tag{8-a}$$

$$\beta_i = -\frac{qN_d}{\varepsilon_{\text{Si}}} + \alpha_i\left(V_{\text{fbi}} - V_{\text{gs}}\right). \tag{8-b}$$

Hence Eq. (8) has a general solution of the form

$$\varphi_{s1}(x) = D_1 e^{-\sqrt{\alpha_1}x} + E_1 e^{-\sqrt{\alpha_1}(L_1-x)} - \sigma_1, \tag{9-a}$$

$$\varphi_{s2}(x) = D_2 e^{-\sqrt{\alpha_2}(x-L_1)} + E_2 e^{-\sqrt{\alpha_2}(L_1+L_2-x)} - \sigma_2, \tag{9-b}$$

$$\varphi_{s3}(x) = D_3 e^{-\sqrt{\alpha_3}(x-L_1-L_2)} + E_3 e^{-\sqrt{\alpha_3}(L-x)} - \sigma_3. \tag{9-c}$$

The coefficients $D_i$, $E_i$, and $\sigma_i$ are detailed in "Appendix A."

## 3.2 Threshold voltage model

The threshold voltage is the value of $V_{\text{gs}}$ at which $\varphi_{s1,\text{min}} = 2\Phi_F$, where $\Phi_F = V_t \ln \frac{N_d}{n_i}$ is the variance between the intrinsic and extrinsic Fermi levels [44].

In the case of the TM-DG structure and due to the coexistence of metal gates M1, M2, and M3 (with different work functions), the minimum of the surface potential $\varphi_{s(i),\text{min}}$ is solely determined by the metal gate with highest work function. The position $x_{\text{min}}$ of the minimum surface potential $\varphi_{s(i),\text{min}}$ can be determined by solving $\frac{d\varphi_{s1}}{dx} = 0$. Thus, we obtain
$x_{\text{min}} = \frac{1}{2\sqrt{\alpha_1}} \ln\left(\frac{D_1}{E_1 \cdot e^{-L_1\sqrt{\alpha_1}}}\right)$. Hence, $\varphi_{s(i),\text{min}}$ is determined as

$$\varphi_{s1,\text{min}} = 2\sqrt{D_1 E_1 e^{-L_1\sqrt{\alpha_1}}} - \delta_1.$$

The final expression for the threshold voltage is therefore

$$V_{\text{th},i} = \frac{-G_i + \sqrt{G_i - 4HK}}{2H}, \tag{10}$$

where

$$G_i = m_1 n_2 + m_2 n_1 - 2p_i, \tag{10-a}$$

$$H = 1 + n_1 n_2, \tag{10-b}$$

$$K = m_1 m_2 + \rho^2. \tag{10-c}$$

The coefficients $m_i$, $n_i$, and $p_i$ are detailed in "Appendix B."

This mathematical model for our device was verified using ATLAS 2-D simulator, where all simulations were realized at room temperature (300 K) [52]. The physical effects used to approximate the numerical model in the analytical model are summarized in Table 2.

**Table 2** Models and methods used for the TCAD simulations of the TM-JL-DG-MOSFET with highly doped source/drain extensions

| Physical effect | TCAD simulation |
|---|---|
| Generation/recombination | Shockley–Read–Hall (SRH) |
| Carrier transport | Drift–diffusion |
| Transverse field | Lombardi constant voltage and temperature (CVT) |
| Carrier mobility | Concentration-based mobility (CONMOB) along with field-dependent mobility (FLD-MOB) |
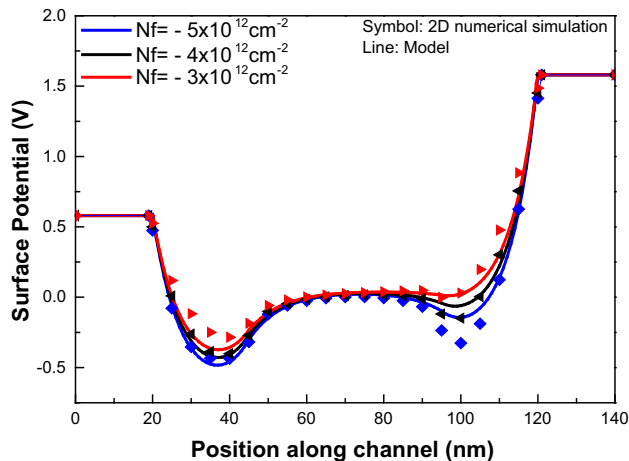


**Fig. 2** Shape of surface potential of TM-DG-DM-JL-MOSFET with highly doped source/drain extensions for different values of charge density (drain voltage $V_{ds} = 1$ V, $V_{gs} = 0$ V)

Note that quantum–mechanical effects (QMEs) were neglected during the simulations and modeling, as they start to dominate for devices having $t_{Si}$ below 5 nm [40].

## 4 Results and discussion

To validate the proposed structure, many simulations were carried out, investigating the impacts of the charge density of DNA molecules and the device dimensions on the surface potential, threshold voltage, sensitivity, and $I_{on}/I_{off}$ ratio.

Figure 2 shows the shape of the surface potential as a function of position along the channel. These simulations were performed using three gate materials with different work functions and different amounts of DNA molecules. The figure clearly shows that the surface potential decreases under the nanogap cavity (the region where the DNA molecules are injected), whereas there is no deformation in the rest of the channel region where the cavity is not formed.

The relation between the surface potential and the charged biomolecules can be explained based on the changes in the

flat-band voltage ($\Delta V_{fb}$) in the cavity region, which depend on the charged biomolecules ($N_f$) as follows: $\Delta V_{fb} = \frac{q N_f}{C_{gap}}$.

Another parameter that was investigated to assess the impact of biomolecules on the device was the threshold voltage, which is an important sensing parameter in such biosensors. Figure 3 depicts the impact of DNA molecules and the nanogap length on the threshold voltage of the TM-DG-DM-JL-MOSFET with highly doped S/D extensions, comparing the results obtained from the developed model with those of the numerical technology computer-aided design (TCAD) simulation.

Figure 3a depicts the variation of the threshold voltage of the TM-DG-DM-JL-MOSFET with highly doped source/drain extensions. These simulations were carried out for different charge densities and several nanogap lengths. It can be seen that the threshold voltage decreases as the charge density of the DNA molecules increases.

Figure 3b plots the variation of the threshold voltage of the considered device as a function of the middle gate length for different values of the charge density. Note that the threshold voltage increases as the middle gate length is decreased.

To investigate the effect of the charge of the biomolecules, the variation of the threshold voltage is also plotted in Fig. 3c. This figure shows corresponding plots for various silicon thicknesses and charge density values. Note that the threshold voltage increases as the silicon thickness is decreased.

Figure 3d depicts the variation in the threshold voltage of the TM-DG-DM-JL-MOSFET with highly doped S/D regions as a function of the nanogap thickness. These simulations were carried out for two different charge densities ($t_{bio}$). It can be clearly seen that there is a small variation in the threshold voltage as the thickness of the hollow regions is increased.

Sensitivity is an important parameter for selection of biosensors, calculated as the shift of the threshold voltage between the presence and absence of DNA molecules in the hollow regions as

$$\Delta V_{th} = V_{th(DNA)} - V_{th(AIR)}$$
$$\Delta V_{TH} = V_{TH(withDNAbiomolecules)}$$
$$- V_{TH(withoutDNAbiomolecules)}. \tag{7}$$

Figure 4a, b depicts the sensitivity when DNA molecules are immobilized in the cavity regions of the TM-DG-DM-JL-MOSFET with highly doped extensions.

Figure 4a reveals that the sensitivity increases as the silicon thickness is decreased (for $t_{Si} = 10$ nm, $\Delta V_{th} = 0.56$ V and for $t_{Si} = 20$ nm, $\Delta V_{th} = 0.33$ V). Conversely, in Fig. 4b, the sensitivity decreases when the length of the cavity region is decreased too; i.e., with $N_f = -3 \times 10^{12}$ cm$^{-2}$, then $L_{gap} = 25$ nm gives $\Delta V_{th} = 480$ mV while $L_{gap} = 20$ nm gives $\Delta V_{th} = 340$ mV.
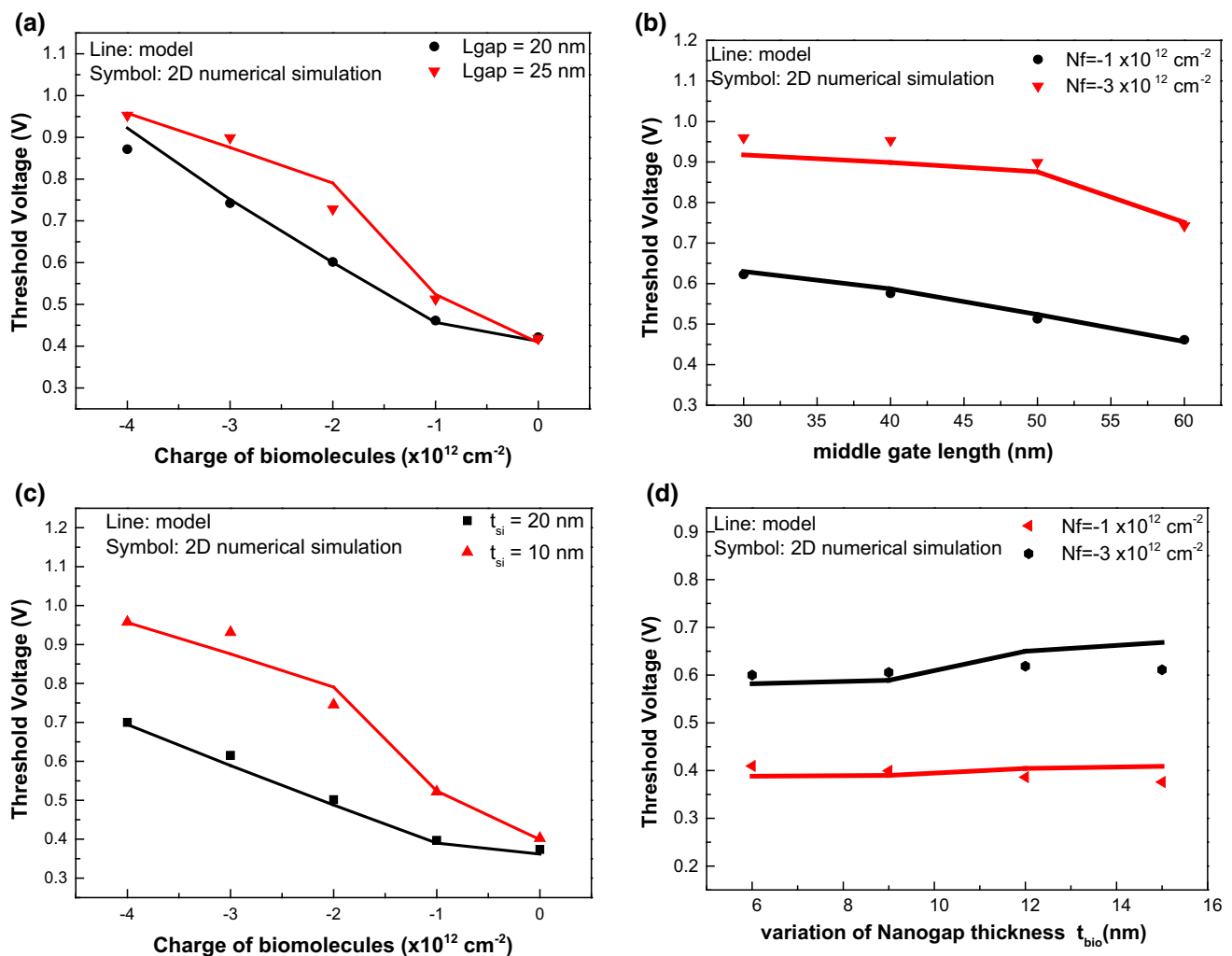
**(a)**



**(b)**



**(c)**



**(d)**



**Fig. 3 a** Variation of the threshold voltage of the TM-DG-DM-JL-MOSFET with highly doped source/drain extensions for different values of the charge density and several lengths of the nanogap ($\varepsilon_{bio}$ = 15, $t_{Si}$ = 10 nm). **b** Variation of the threshold voltage of the TM-DG-DM-JL-MOSFET with highly doped source/drain extensions for different values of the charge density and several lengths of the middle gate. **c** Variation of the threshold voltage of the TM-DG-DM-JL-MOSFET with highly doped source/drain extensions for different values of the charge density for several thicknesses of silicon. **d** Variation of the threshold voltage of the TM-DG-DM-JL-MOSFET with highly doped source/drain extensions for different values of the nanogap thickness $t_{bio}$ and several charge densities ($\varepsilon_{bio}$ = 13, $t_{Si}$ = 10 nm)

Figure 4c plots the variation of the sensitivity of the TM-DG-DM-JL-MOSFET with highly doped source/drain extensions for several middle gate lengths and different values of the charge density. The middle gate length was varied from 30 to 60 nm. The results clearly show that the sensitivity with a longer middle gate was low compared with that obtained for short middle gate length; nevertheless, the functionality of the considered biosensor remains acceptable.

Figure 4d depicts the variation of the sensitivity of the device under study for several nanogap cavity thicknesses and different values of the charge density. Note from this curve that a slight variation occurs in terms of sensitivity as the nanogap cavity thickness is increased.

Figures 5 and 6 show simulation results for the transfer characteristic and $I_{on}/I_{off}$ ratio for different values of the charge density for the TM-DG-DM-JL-MOSFET with highly doped extensions. These simulations were performed using the TCAD simulator.

Figure 5 plots the drain current as a function of the gate voltage for different charge density values. The results clearly show that, as the charge density of the DNA molecules increases, the on/off currents decrease.

The $I_{on}/I_{off}$ ratio is another useful parameter for assessment of the sensitivity of biosensors. Figure 6 shows the impact of the DNA molecule density on the $I_{on}/I_{off}$ ratio of the TM-DG-DM-JL-MOSFET with highly doped source/drain extensions for different gate oxide materials,
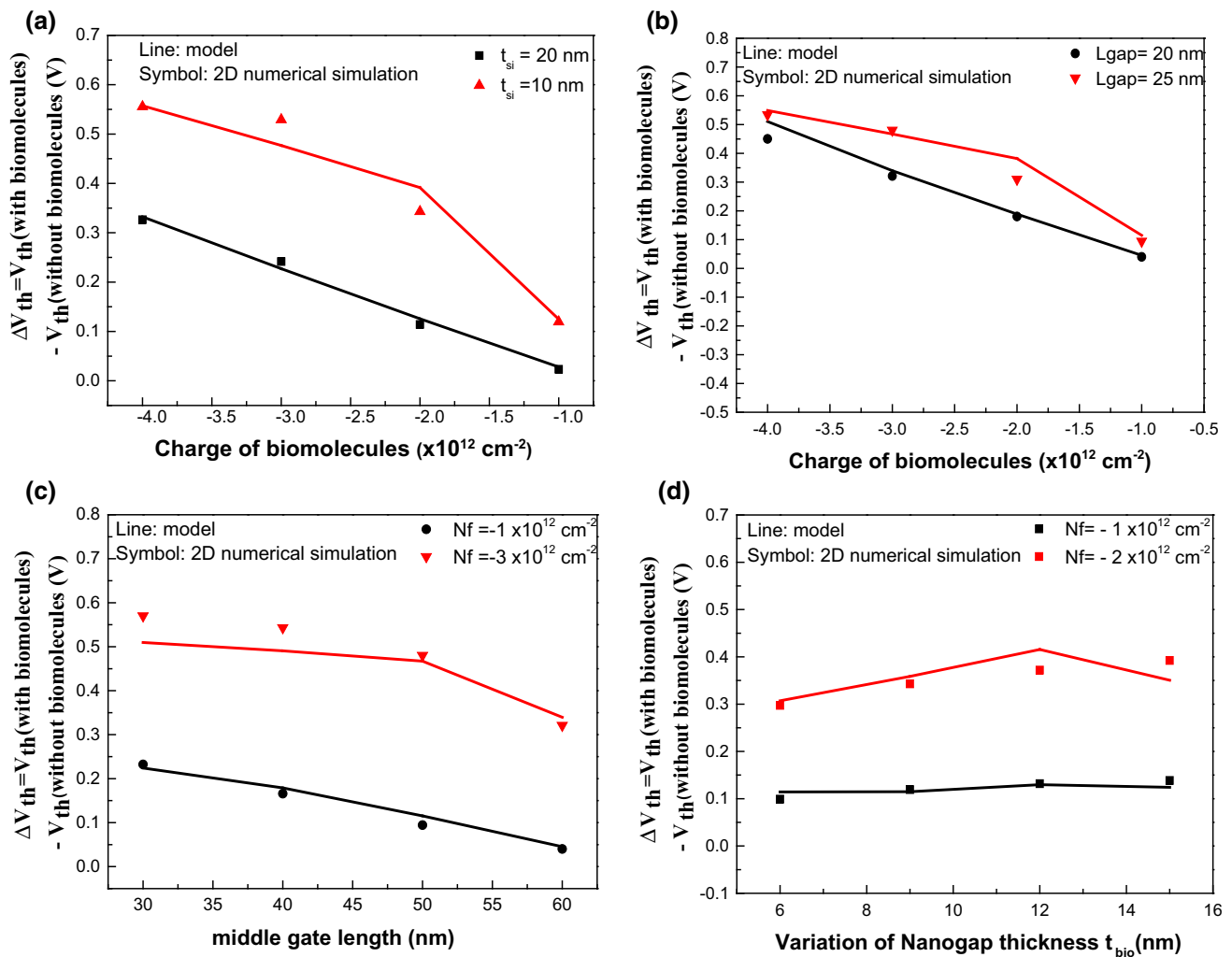
**Fig. 4 a** Variation of the sensitivity of the TM-DG-DM-JL-MOSFET with highly doped source/drain extensions for different values of the charge density and several thicknesses of silicon ($K_{bio} = 13$, $t_{bio} = 9$ nm). **b** Variation of the sensitivity of the TM-DG-DM-JL-MOSFET with highly doped source/drain extensions for different values of the charge density and various lengths of the nanogap cavity ($K_{bio} = 15$, $t_{bio} = 9$ nm). **c** Variation of the sensitivity of the TM-DG-DM-JL-MOSFET with highly doped source/drain extensions for several lengths of middle gate and different values of the charge density ($K_{bio} = 15$, $t_{bio} = 9$ nm). **d** Variation of the sensitivity of the TM-DG-DM-JL-MOSFET with highly doped source/drain extensions for several thicknesses of the nanogap cavity and different values of charge density ($K_{bio} = 13$)

namely $Al_2O_3$ and $SiO_2 + TiO_2$. When DNA molecules are immobilized in the cavity region, use of $SiO_2$ and $TiO_2$ as gate oxide materials allows an increase in the $I_{on}/I_{off}$ ratio compared with the use of $Al_2O_3$.

## 5 Comparison of TM-DG-DM-JL-MOSFET with SM-DM-JL-MOSFET

This section compares the sensitivity of the developed device with that of an SM-DG-DM-JL-MOSFET [37] of similar dimensions.

The sensitivity of both devices is presented in Table 3. These results clearly show that the TM-DG-DM-JL-MOSFET with highly doped extensions provides high sensitivity with presence of DNA molecules in the nanogap cavity compared with the SM-DG-DM-JL-MOSFET.

## 6 Conclusions

Analytical and numerical modeling studies were carried out to analyze the sensitivity of a DG-DM-JL-MOSFET-based biosensor depending on its physical and electrical parameters. To assess the impact of DNA molecules (essential
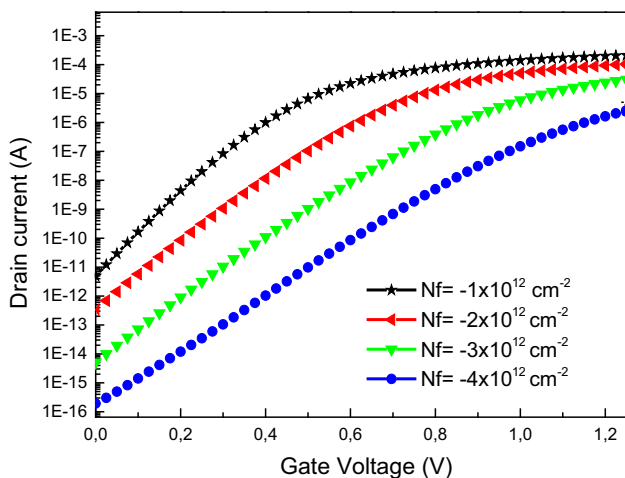
**Fig. 5** Variation of the drain current as a function of the gate voltage for the TM-DG-DM-JL-MOSFET with highly doped source/drain extensions for different values of the charge density ($K_{bio} = 15$, $t_{bio} = 9\,nm$, and $t_{Si} = 10\,nm$)



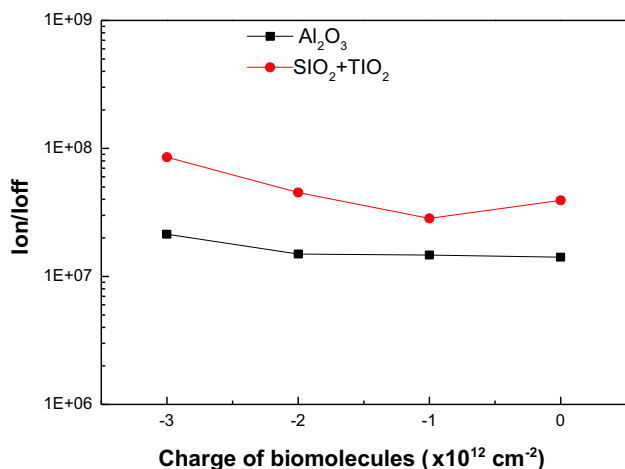**Fig. 6** Variation of the $I_{on}/I_{off}$ ratio for different values of the charge density for the TM-DG-DM-JL-MOSFET with highly doped source/drain extensions for different gate oxide materials ($Al_2O_3$ and $SiO_2 + TiO_2$)

biomolecules in Nature), gate engineering and highly doped source/drain extensions of the DG-DM-JL-MOSFET were considered. It is noteworthy that this structure is the most useful to achieve the typical biosensing characteristic.

The investigated parameters included the surface potential, threshold voltage, sensitivity, transfer characteristic, and $I_{on}/I_{off}$ ratio as functions of the biomolecule charge density and dimensional parameters of the biosensor. The results demonstrate the superiority of the TM-DG-DM-JL-MOSFET over the SM-DM-JL-MOSFET based on a comparison of the sensitivity of each device. The TM-DG-DM-JL-MOSFET with highly doped extensions permits detection of DNA molecules with sensitivity almost 50 % higher compared with the SM-DG-DM-JL-MOSFET structure.

The results presented herein prove the effectiveness of the proposed design over the conventional SM-DM-JL-MOSFET. The insight offered by this investigation makes the TM-DG-DM-JL-MOSFET with highly doped extensions a potential candidate for use in biosensing applications.

## Appendix A

$$\sigma_i = -\frac{\beta_i}{\alpha_i},$$

$$D_1 = \frac{(V_{bi} - \sigma_1) - (V_1 - \sigma_1)e^{-L_1\sqrt{\alpha_1}}}{1 - e^{-2L_1\sqrt{\alpha_1}}},$$

$$E_1 = \frac{(V_1 - \sigma_1) - (V_{bi} - \sigma_1)e^{-L_1\sqrt{\alpha_1}}}{1 - e^{-2L_1\sqrt{\alpha_1}}},$$

$$D_2 = \frac{(V_1 - \sigma_2) - (V_2 - \sigma_2)e^{-L_2\sqrt{\alpha_2}}}{1 - e^{-2L_2\sqrt{\alpha_2}}},$$

$$E_2 = \frac{(V_2 - \sigma_2) - (V_1 - \sigma_2)e^{-L_2\sqrt{\alpha_2}}}{1 - e^{-2L_2\sqrt{\alpha_2}}},$$

$$D_3 = \frac{(V_2 - \sigma_3) - (V_{bi} + V_{ds} - \sigma_3)e^{-L_3\sqrt{\alpha_3}}}{1 - e^{-2L_3\sqrt{\alpha_3}}},$$

where $V_{bi}$ is the built-in potential, $V_1$ and $V_2$ are intermediate potentials, obtained by maintaining the continuity of the potential at the interface between region I, II, and III. Thus, we obtain

**Table 3** Comparison of the TM-JL-DG-MOSFET with highly doped source/drain extensions versus the SM-DM-JL-MOSFET

| Parameter | Sensitivity of SM-DM-JL-MOSFET (V) | Sensitivity of TM-DG-DM-JL-MOSFET (V) |
|---|---|---|
| $N_f = -4 \times 10^{12}$ cm$^{-2}$ $t_{Si} = 10$ nm, $L_{gap} = 25$ nm, $t_{bio} = 9$ nm, $L = 100$ nm | −0.25 [37] | 0.55 |
| $N_f = -2 \times 10^{12}$ cm$^{-2}$ $t_{bio} = 14$ nm, $L_{gap} = 25$ nm | −0.08 [37] | 0.35 |

$$A_1 V_1 + B_1 V_2 = F_1,$$

$$A_2 V_1 + B_2 V_2 = F_2,$$

where

$$A_1 = \frac{e^{2L_1\sqrt{\alpha_1}} + 1}{e^{2L_1\sqrt{\alpha_1}} - 1} + \frac{e^{2L_2\sqrt{\alpha_2}} + 1}{e^{2L_2\sqrt{\alpha_2}} - 1},$$

$$B_1 = \frac{-2}{e^{L_2\sqrt{\alpha_2}} - e^{-L_2\sqrt{\alpha_2}}},$$

$$F_1 = V_{\text{bi}}\left(\frac{2}{e^{L_1\sqrt{\alpha_1}} - e^{-L_1\sqrt{\alpha_1}}}\right)$$
$$+ \delta_1\left(\frac{2}{e^{L_1\sqrt{\alpha_1}} - e^{-L_1\sqrt{\alpha_1}}} - \frac{e^{2L_1\sqrt{\alpha_1}} + 1}{e^{2L_1\sqrt{\alpha_1}} - 1}\right)$$
$$+ \delta_2\left(\frac{2}{e^{L_2\sqrt{\alpha_2}} - e^{-L_2\sqrt{\alpha_2}}} - \frac{e^{2L_2\sqrt{\alpha_2}} + 1}{e^{2L_2\sqrt{\alpha_2}} - 1}\right),$$

$$A_2 = \frac{-2}{e^{L_2\sqrt{\alpha_2}} - e^{-L_2\sqrt{\alpha_2}}},$$

$$B_2 = \frac{e^{2L_2\sqrt{\alpha_2}} + 1}{e^{2L_2\sqrt{\alpha_2}} - 1} + \frac{e^{2L_3\sqrt{\alpha_3}} + 1}{e^{2L_3\sqrt{\alpha_3}} - 1},$$

$$F_2 = (V_{\text{bi}} + V_{\text{ds}})\left(\frac{2}{e^{L_3\sqrt{\alpha_3}} - e^{-L_3\sqrt{\alpha_3}}}\right)$$
$$+ \delta_2\left(\frac{2}{e^{L_2\sqrt{\alpha_2}} - e^{-L_2\sqrt{\alpha_2}}} - \frac{e^{2L_2\sqrt{\alpha_2}} + 1}{e^{2L_2\sqrt{\alpha_2}} - 1}\right)$$
$$+ \delta_3\left(\frac{2}{e^{L_3\sqrt{\alpha_3}} - e^{-L_3\sqrt{\alpha_3}}} - \frac{e^{2L_3\sqrt{\alpha_3}} + 1}{e^{2L_3\sqrt{\alpha_3}} - 1}\right).$$

Using Crammer's rule, it is possible to obtain the values of the intermediate potential $V_1$ and $V_2$ at the interfaces of regions I, II, and III as follows:

$$V_1 = \frac{\begin{vmatrix} F_1 & B_1 \\ F_2 & B_2 \end{vmatrix}}{\begin{vmatrix} A_1 & B_1 \\ A_2 & B_2 \end{vmatrix}} = \frac{F_1 B_2 - F_2 B_1}{A_1 B_2 - A_2 B_1},$$

$$V_2 = \frac{\begin{vmatrix} A_1 & F_1 \\ A_2 & F_2 \end{vmatrix}}{\begin{vmatrix} A_1 & B_1 \\ A_2 & B_2 \end{vmatrix}} = \frac{A_1 F_2 - F_1 A_2}{A_1 B_2 - A_2 B_1}.$$

## Appendix B

$$m_1 = 2 \times e^{-L_1\sqrt{\alpha_1}}\left(\frac{(V_{\text{bi}} + r_i)e^{-L_1\sqrt{\alpha_1}} - (V_{s1} + r_i)}{1 - e^{-2L_1\sqrt{\alpha_1}}}\right),$$

$$m_2 = 2 \times \frac{(V_{\text{bi}} + r_i) - (V_{s1} + r_i)e^{-L_1\sqrt{\alpha_1}}}{1 - e^{-2L_1\sqrt{\alpha_1}}},$$

$$n_1 = 2 \times e^{-L_1\sqrt{\alpha_1}}\left(\frac{1 - V_{s2} - e^{-L_1\sqrt{\alpha_1}}}{1 - e^{-2L_1\sqrt{\alpha_1}}}\right),$$

$$n_2 = 2 \times \frac{e^{-L_1\sqrt{\alpha_1}} - V_{s2}e^{-L_1\sqrt{\alpha_1}} - 1}{1 - e^{-2L_1\sqrt{\alpha_1}}},$$

$$V_{s1} = \frac{C_{11}B_2 - C_{21}B_1}{A_1 B_2 - A_2 B_1}, \quad V_{s2} = \frac{C_{12}B_2 - C_{22}B_1}{A_1 B_2 - A_2 B_1},$$

$$p_i = \frac{qN_f}{C_i} + V_{\text{fbi}} + 2\left(V_t ln\frac{N_d}{n_i}\right),$$

$$C_{11} = \left(\frac{2}{e^{L_2\sqrt{\alpha_2}} - e^{-L_2\sqrt{\alpha_2}}} - \frac{e^{2L_2\sqrt{\alpha_2}} + 1}{e^{2L_2\sqrt{\alpha_2}} - 1}\right)r_2$$
$$+ \left(\frac{2}{e^{L_1\sqrt{\alpha_1}} - e^{-L_1\sqrt{\alpha_1}}} - \frac{e^{2L_1\sqrt{\alpha_1}} + 1}{e^{2L_1\sqrt{\alpha_1}} - 1}\right)r_1$$
$$+ V_{\text{bi}}\left(\frac{2}{e^{L_1\sqrt{\alpha_1}} - e^{-L_1\sqrt{\alpha_1}}}\right),$$

$$C_{21} = \frac{e^{2L_2\sqrt{\alpha_2}} + 1}{e^{2L_2\sqrt{\alpha_2}} - 1} - \frac{2}{e^{L_2\sqrt{\alpha_2}} - e^{-L_2\sqrt{\alpha_2}}} + \frac{e^{2L_1\sqrt{\alpha_1}} + 1}{e^{2L_1\sqrt{\alpha_1}} - 1}$$
$$- \frac{2}{e^{L_1\sqrt{\alpha_1}} - e^{-L_1\sqrt{\alpha_1}}},$$

$$C_{12} = \left(\frac{2}{e^{L_2\sqrt{\alpha_2}} - e^{-L_2\sqrt{\alpha_2}}} - \frac{e^{2L_2\sqrt{\alpha_2}} + 1}{e^{2L_2\sqrt{\alpha_2}} - 1}\right)r_2$$
$$+ \left(\frac{2}{e^{L_3\sqrt{\alpha_3}} - e^{-L_3\sqrt{\alpha_3}}} - \frac{e^{2L_3\sqrt{\alpha_3}} + 1}{e^{2L_3\sqrt{\alpha_3}} - 1}\right)r_3$$
$$+ (V_{\text{bi}} + V_{\text{ds}})\left(\frac{2}{e^{L_3\sqrt{\alpha_3}} - e^{-L_3\sqrt{\alpha_3}}}\right),$$

$$C_{22} = \frac{e^{2L_2\sqrt{\alpha_2}} + 1}{e^{2L_2\sqrt{\alpha_2}} - 1} - \frac{2}{e^{L_2\sqrt{\alpha_2}} - e^{-L_2\sqrt{\alpha_2}}} + \frac{e^{2L_3\sqrt{\alpha_3}} + 1}{e^{2L_3\sqrt{\alpha_3}} - 1} - \frac{2}{e^{L_3\sqrt{\alpha_3}} - e^{-L_3\sqrt{\alpha_3}}},$$

$$r_i = -\frac{qN_d}{\varepsilon_{Si}} + V_{fbi}, \quad i = 1, 2, 3.$$

# References

1. Kim, J.M., Jha, S.K., Chand, R., Lee, D.H., Kim, Y.S.: Flexible pentacene thin film transistors as DNA hybridization sensor. In: IEEE International Conference on Nano/Micro Engineered and Molecular Systems. Proceeding, Kaohsiung, Taiwan, pp. 421–424 (2011)

2. Patolsky, F., Lichtenstein, A., Willner, I.: Detection of single-base DNA mutations by enzyme-amplified electronic transduction. Nat. Biotechnol. **19**, 253–257 (2001)

3. Nam, J.M., Stoveva, S.I., Mirkin, C.A.: Bio-bar-code-based DNA detection with PCR-like sensitivity. J. Am. Chem. Soc. **126**, 5932–5933 (2004)

4. Ramsay, G.: DNA chip: state-of-the art. Nat. Biotechnol. **16**, 40–44 (1998)

5. Marshall, A., Hhodgson, J.: DNA chips: an array of possibilities. Nat. Biotechnol. **16**, 27–31 (1998)

6. Pividori, M.I., Merkoci, A., Alegret, S.: Electrochemical genosensor design: immobilisation of oligonucleotides onto transducer surfaces and detection methods. Biosens. Bioelectron. **15**, 291–303 (2000)

7. Kim, C.H., Jung, C., Park, H.G., Choi, Y.K.: Novel dielectric modulated field-effect transistor for label-free DNA detection. Biochip J. **2**(2), 127–134 (2008)

8. Jang, D.Y., et al.: Sublithographic vertical gold nano-gap for label-free electrical detection of protein–ligand binding. J. Vac. Sci. Technol. **B25**, 443–447 (2007)

9. Peng, H., et al.: Label-free electrochemical DNA sensor based on functionalized conducting copolymer. Biosens. Bioelectron. **20**, 1821–1828 (2005)

10. Chen, J.-C., Chou, J.-C., Sun, T.-P., Hsiung, S.-K.: Portable urea biosensor based on the extended-gate field effect transistor. Sens. Actuators B Chem. **91**(1–3), 180–186 (2003)

11. Kim, D.-S., Park, J.-E., et al.: An extended gate FET-based biosensor integrated with a Si microfluidic channel for detection of protein complexes. Sens. Actuator B Chem. **117**(2), 488–494 (2006)

12. Schöning, M.J., Poghossian, A.: Recent advances in biologically sensitive field-effect transistors (BioFETs). Analyst **127**(9), 1137–1151 (2002)

13. Bergveld, P.: Thirty years of ISFETOLOGY: what happened in the past 30 years and what may happen in the next 30 years. Sens. Actuators B Chem. **88**(1), 1–20 (2003)

14. Park, K.Y., Choi, S.B., Lee, M., Sohn, B.K., Choi, S.Y.: ISFET glucose sensor system with fast recovery characteristics by employing electrolysis. Sens. Actuators B Chem. **83**(1–3), 90–97 (2002)

15. Phogossian, A., Schoning, J., et al.: An ISFET-based penicillin sensor with high sensitivity, low detection limit and long lifetime. Sens. Actuators B Chem. **76**(1–3), 519–526 (2001)

16. Choi, J.M., Han, J.W., Choi, S.J., Choi, Y.K.: Analytical modeling of a nanogap-embedded FET for application as a biosensor. IEEE Trans. Electron Devices **57**(12), 3477–3484 (2010)

17. Cui, Y., Wei, Q., Park, H., Lieber, C.M.: Nanowire nanosensors for highly sensitive and selective detection of biological and chemical species. Science **293**(5533), 1289–1292 (2001)

18. Stern, E., Klemic, J.F., et al.: Label-free immunodetection with CMOS-compatible semiconducting nanowires. Nature **445**(7127), 519–523 (2007)

19. Li, Z., Chen, Y., et al.: Sequence-specific label-free DNA sensors based on silicon nanowires. Nano Lett. **4**(2), 245–247 (2004)

20. Hahm, J., Lieber, C.M.: Direct ultrasensitive electrical detection of DNA and DNA sequence variations using nanowire nanosensors. Nano Lett. **4**(1), 51–54 (2004)

21. Curreli, M., Zhang, R., et al.: Real-time, label-free detection of biological entities using nanowire-based FETs. IEEE Trans. Nanotechnol. **7**(6), 651–667 (2008)

22. Qi, P., Vermesh, O., Grecu, M., et al.: Toward large arrays of multiplex functionalized carbon nanotube sensors for highly sensitive and selective molecular detection. Nano Lett. **3**(3), 347–351 (2003)

23. Star, A., Tu, E., Niemann, J., et al.: Label-free detection of DNA hybridization using carbon nanotube network field-effect transistors. Proc. Natl. Acad. Sci. USA **103**(4), 921–926 (2006)

24. Martinez, M.T., Tseng, Y.-C., et al.: Label-free DNA biosensors based on functionalized carbon nanotube field effect transistors. Nano Lett. **9**(2), 530–536 (2009)

25. Im, H., Huang, X.-J., Gu, B., Choi, Y.-K.: A dielectric-modulated field-effect transistor for biosensing. Nat. Nanotechnol. **2**(7), 430–434 (2007)

26. Kim, C.-H., Jung, C., Lee, K.-B., Park, H.G., Choi, Y.-K.: Label-free DNA detection with a nanogap embedded complementary metal oxide semiconductor. Nanotechnology **22**(13), 135502-1–135502-5 (2011)

27. Gu, B., Park, T.J., Ahn, J.-H., Huang, X.-J., Lee, S.Y., Choi, Y.-K.: Nanogap field-effect transistor biosensors for electrical detection of avian influenza. Small **5**(21), 2407–2412 (2009)

28. Im, M., Ahn, J.-H., Han, J.-W., Park, T.J., Lee, S.Y., Choi, Y.K.: Development of a point-of-care testing platform with a nanogap-embedded separated double-gate field effect transistor array and its readout system for detection of avian influenza. IEEE Sens. J. **11**(2), 351–360 (2011)

29. Kim, C.-H., Jung, C., Park, H.G., Choi, Y.-K.: Novel dielectric-modulated field-effect transistor for label-free DNA detection. Biochip J. **2**(2), 127–134 (2008)

30. Kim, S., Baek, D., Kim, J.-Y., Choi, S.-J., Seol, M.-L., Choi, Y.-K.: A transistor-based biosensor for the extraction of physical properties from biomolecules. Appl. Phys. Lett. **101**(7), 073703-1–073703-4 (2012)

31. Kim, S., Ahn, J.-H., Park, T.J., Lee, S.Y., Choi, Y.-K.: A biomolecular detection method based on charge pumping in a nanogap embedded field-effect-transistor biosensor. Appl. Phys. Lett. **94**(24), 243903 (2009)

32. Kim, C.-H., Ahn, J.-H., Lee, K.-B., Jung, C., Park, H.G., Choi, Y.-K.: A new sensing metric to reduce data fluctuations in a nanogap embedded field-effect transistor biosensor. IEEE Trans. Electron Devices **59**(10), 2825–2831 (2012)

33. Kim, S., Ahn, J.-H., Park, T.J., Lee, S.Y., Choi, Y.-K.: Charge pumping technique to analyze the effect of intrinsically retained charges and extrinsically trapped charges in biomolecules by use of a nanogap embedded biotransistor. Appl. Phys. Lett. **96**(5), 053701 (2010)

34. Kannan, N., Kumar, M.J.: Dielectric-modulated impact-ionization MOS transistor as a labelfree biosensor. IEEE Electron Device Lett. **34**(12), 1575–1577 (2013)

35. Kim, S., Ahn, J.H., Park, T.J., Lee, S.Y., Choi, Y.K.: Comprehensive study of a detection mechanism and optimization strategies to improve sensitivity in a nanogap-embedded biotransistor. J. Appl. Phys. **107**(11), 114705 (2010)

36. Kanungo, S., Chattopadhyay, S., Gupta, P.S., Rahaman, H.: Comparative performance analysis of the dielectrically modulated full gate and short-gate tunnel FET-based biosensors. IEEE Trans. Electron Devices **62**(3), 994–1001 (2015)

37. Ajay, S., Narang, R., Saxena, M., Gupta, M.: Investigation of dielectric modulated (DM) double gate (DG) junctionless MOS-FETs for application as a bio-sensors. Superlattices Microstruct. **85**, 557–572 (2015)

38. Parihar, M.S., Kranti, A.: Enhanced sensitivity of double gate junctionless transistor architecture for bio-sensing applications. Nanotechnology **26**, 145201 (2015)

39. Chakraborty, A., Sarkar, A.: Analytical modeling and sensitivity analysis of dielectric-modulated junction-less gate stack surrounding gate MOSFET (JLGS-SRG) for application as biosensor. J. Comput. Electron. **16**, 556–567 (2017)

40. Chebaki, E., Djeffal, F., Ferhati, H., Bentrcia, T.: Improved analog/RF performance of double gate junctionless MOSFET using both gate material engineering and drain/source extensions. Superlattices Microstruct. **92**, 80–91 (2016)

41. Razavi, P., Orouji, A.A.: Dual material gate oxide stack symmetric double gate MOSFET: improving short channel effects of nanoscale double gate MOSFET. In: Electronics Conference, 2008. BEC 2008. 11th International Biennial Baltic, IEEE, pp. 83–86 (2008)

42. Ahangari, Z.: Performance assessment of dual material gate dielectric modulated nanowire junctionless MOSFET for ultrasensitive detection of biomolecules. RSC Adv. **6**(92), 89185–89191 (2016)

43. Long, W., Ou, H., Kuo, J.M., Chin, K.K.: Dual material gate (DMG) field effect transistor. IEEE Trans. Electron Devices **46**, 865–870 (1999)

44. Kumar, M.J., Chaudhary, A.: Two-dimensional analytical modeling of fully depleted DMG SOI MOS-FET and evidence for diminished SCEs. IEEE Trans. Electron Devices **51**(4), 569–574 (2004)

45. Jouri, M., ShahrokhAbadi, M.H.: Analytical investigation of triple-material cylindrical gate surrounded (TM-CGS) MOSFETs with high-K material oxide. Phys. J. **1**(3), 325–330 (2015)

46. Baral, B., Das, A.K., De, D., Sarkar, A.: An analytical model of triple-material double gate metal oxide semiconductor field-effect transistor to suppress short channel effects. Int. J. Numer. Model. **29**, 47–62 (2015)

47. Razavi, P., Orouji, A.A.: Nanoscale triple material double gate (TM-DG) MOSFET for improving short channel effects. In: Advances in Electronics and Micro-electronics, 2008, Valencia, Spain, 29 September–4 October (2008)

48. Tiwari, P.K., Dubey, S., Singh, M., Jit, S.: A two-dimensional analytical model for threshold voltage of short-channel triple-material-gate metal-oxide-semiconductor field-effect transistors. J. Appl. Phys. **108**, 074508 (2010)

49. Dubey, S., Santra, A., Saramekala, G., Kumar, M., Tiwari, P.K.: An analytical threshold voltage model for triple-material cylindrical gate-all-around (TM-CGAA) MOSFETs. IEEE Trans. Electron Nanotechnol. **12**(5), 766–774 (2013)

50. Kinsella, J.M., Ivanisevic, A.: Taking charge of biomolecules. Nat. Nanotechnol. **2**, 596–597 (2007)

51. Young, K.K.: Short-channel effect in fully depleted SOI MOS-FET's. IEEE Trans. Electron Devices **36**(2), 399 (1989)

52. ATLAS User Manual: Device Simulation Software (2012)